J. Phys. B: At. Mol. Opt. Phys. **33** (2000) 4017–4031. Printed in the UK PII: S0953-4075(00)50592-6

Structure of binary Bose–Einstein condensates

Marek Trippenbach†‡, Krzysztof Góral§, Kazimierz Rzążewski§, Boris Malomed‖ and Y B Band†

† Departments of Chemistry and Physics, Ben-Gurion University of the Negev, Beer-Sheva, Israel 84105

‡ Institute of Experimental Physics, Optics Division, Warsaw University, ul. Hoża 69, Warsaw 00-681, Poland

§ Center for Theoretical Physics and College of Science, Polish Academy of Sciences, Al. Lotników 32/64, Warsaw 02-668, Poland

‖ Department of Interdisciplinary Studies, Faculty of Engineering, Tel-Aviv University, Tel-Aviv, Israel 69978

Received 27 April 2000

Abstract. We identify all possible classes of solutions for two-component Bose–Einstein condensates (BECs) within the Thomas–Fermi (TF) approximation and check these results against numerical simulations of the coupled Gross–Pitaevskii equations (GPEs). We find that they can be divided into two general categories. The first class contains solutions with a region of overlap between the components. The other class consists of non-overlapping wavefunctions and also contains solutions that do not possess the symmetry of the trap. The chemical potential and average energy can be found for both classes within the TF approximation by solving a set of coupled algebraic equations representing the normalization conditions for each component. A ground state minimizing the energy (within both classes of states) is found for a given set of parameters characterizing the scattering length and confining potential. In the TF approximation, the ground state always shares the symmetry of the trap. However, a full numerical solution of the coupled GPEs, incorporating the kinetic energy of the BEC atoms, can sometimes select a broken-symmetry state as the ground state of the system. We also investigate effects of finite-range interactions on the structure of the ground state.

1. Introduction

Phase transitions and the coexistence of different phases in multi-component systems are of great importance to many areas of physics, chemistry and biology. An ideal system to study these phenomena is a multi-component dilute atomic gas Bose–Einstein condensate (BEC) mixture at zero temperature, due to the simplicity of its theoretical description. The mean-field approximation provides an excellent description of these systems. Other multi-component systems cannot be understood as well as these BEC mixtures, because their density is generally much higher, and the delta-function pseudopotential, used to describe interactions between atoms in BEC, is not appropriate for them. Instead, a true microscopic interaction potential must be employed to adequately describe such systems, hence modelling them is much harder.

Multi-component BECs have been extensively studied over the last few years [1–10]. These studies have been motivated by experimental work performed by the JILA [11] and MIT [12] groups. Many interesting effects have been determined experimentally and predicted theoretically, including topological properties of the ground and excited states, phase transitions

0953-4075/00/194017+15$30.00

and symmetry breaking [5] effects produced by a phase difference between components [6], stability properties [7], Josephson-type oscillations [8], four-wave mixing [13] and trapping of boson–fermion and fermion–fermion systems [14]. Nevertheless, many features of BEC mixtures remain to be explored by theorists and experimentalists.

A large variety of different species can be used to produce mixtures of condensed bosons. Mixtures of two different elements, or of different isotopes of the same element, or simply different hyperfine states of the same atom [11, 12] can be considered. Simulating experimental results for BEC binary mixtures requires knowledge of the scattering lengths of the atoms involved. To the extent that the values of the scattering lengths are known with insufficient accuracy, a full classification of different states is necessary within the range of possible values. This is also necessary in the context of tuning the scattering length, as can be done by means of changing the external magnetic field near Feshbach resonances [15]. By varying the scattering length, one can study phase transitions to states that break the symmetry of the trapping potential. Such states are known in the literature, and they were observed in the JILA experiment [11].

The classification of two-component condensates can also be carried out in systems with interconversion of components ('chemical reactions' between them), as in the case of an atom–molecule condensate, where the conserved quantity is the number of atoms plus twice the number of molecules (the number of atoms and the number of molecules are not separately conserved). A mathematical model of the latter system can be formulated in terms of two coupled Gross–Pitaevskii equations (GPEs), which contain, in addition to the familiar cubic self- and cross-interaction nonlinear terms, quadratic terms that account for the 'chemistry' (i.e. the interconversion) [16]. In particular, an interesting prediction of the model is that a 'soliton' state, i.e. a stationary self-supported condensate cloud (similar to 'light bullets' in nonlinear optics [17]), may exist without any trapping potential being present [16].

Many aspects of binary condensate mixtures have been treated in the literature, using various (mostly numerical) methods in order to predict results for various experimental set-ups (see, e.g., [2–4]). Nevertheless, a general classification of all the ground-state solutions is not yet available. This is understandable in view of many control parameters present in the models (three scattering lengths, particle numbers for both components and characteristics of the trap). A very general and elegant, but not explicit, algorithm for determining ground-state shapes has been proposed by Ho and Shenoy [1]. Here we start with the same goal in mind, but also with the intention of providing a maximally straightforward and analytic set of expressions for the ground-state wavefunctions and energies of atomic gas BEC mixtures.

We use a computational method simulating the evolution of two-component GPEs in imaginary time [2] in order to study phase separation of components in BEC mixtures. Results produced by this method are compared with analytical predictions based upon the Thomas–Fermi (TF) approximation applied to two-component GPEs. We analyse the changes in the structure of separated phase BEC mixtures with the variation of the s-wave scattering lengths and atom numbers. The changes can be predicted and understood using a simple TF approximation, which includes equations obtained from normalization conditions for both components. The TF picture is compared with solutions obtained using numerically simulated GPE evolution in imaginary time, which includes the kinetic energy of atoms neglected in the TF approximation. We find that, for the simple case of a spherically symmetric harmonic trapping potential, many spherically symmetric phase-separated geometries are possible, depending on the ratios of the self- and cross-s-wave scattering lengths for atomic collisions. In the TF approximation, symmetry-broken phase-separated geometries (i.e. those whose symmetry is lower than that of the trap) are always energetically higher in energy than those with unbroken symmetry. Nevertheless, numerical simulations in imaginary time show that a

lower-symmetry state may be the lowest-energy eigenstate, and thus determine a ground state of the system. Our method may be generalized to include a finite-range interaction between atoms. In the last section of the paper we study, by means of direct numerical simulations, how such interactions affect the geometry and shape of the ground state.

2. Mean-field description of two-component Bose–Einstein mixtures

In this paper, we concentrate on stationary states of BEC mixtures (not their dynamics), therefore we start with the time-independent coupled GPEs, written in the standard notation:

$$\left(-\mu_1 - \frac{\hbar^2\nabla^2}{2m_1} + V_1(\boldsymbol{r}) + U_{11}|\psi_1(\boldsymbol{r},t)|^2 + U_{12}|\psi_2(\boldsymbol{r},t)|^2\right)\psi_1(\boldsymbol{r},t) = 0 \quad (1)$$

$$\left(-\mu_2 - \frac{\hbar^2\nabla^2}{2m_2} + V_2(\boldsymbol{r}) + U_{12}|\psi_1(\boldsymbol{r},t)|^2 + U_{22}|\psi_2(\boldsymbol{r},t)|^2\right)\psi_2(\boldsymbol{r},t) = 0. \quad (2)$$

Here $\mu_{1,2}$ are chemical potentials of the two species and $V_{1,2}(\boldsymbol{r})$ are two isotropic parabolic trapping potentials, i.e.

$$V_j(\boldsymbol{r}) = (m_j/2)\omega_j^2 r^2 \qquad j = 1, 2 \quad (3)$$

ω_j being the corresponding frequencies of harmonic oscillations of a trapped particle. Furthermore, $U_{ij} \equiv \left(4\pi\hbar^2/m_{ij}\right)a_{ij}$ are atom–atom interaction strengths, proportional to the s-wave scattering lengths a_{11}, a_{22} and a_{12} for the 1 + 1, 2 + 2 and 1 + 2 collisions, respectively, where 1 and 2 enumerate the components, and $m_{ij} = m_i$ if $i = j$ and $m_{ij} = m_1 m_2/(m_1 + m_2)$ if $i \neq j$. For simplicity, in the numerical calculations presented here we take $m_1 = m_2 \equiv m$ and assume that the magnetic moments of atoms belonging to the different components are equal, so that the corresponding trapping potentials are equal too, $\omega_1 = \omega_2 \equiv \omega$, but this condition as well as the spherical symmetry condition may be readily relaxed by means of rescaling variables. Furthermore, we assume that the scattering lengths are real, i.e. we assume that collisions are not lossy. We also assume that all the scattering lengths for both different and alike atoms are positive; otherwise, the classification of the possible states becomes very cumbersome.

Our calculations were carried out, simulating the evolution in the *time-dependent* GPEs in imaginary time [2], so as to let the solution relax to the ground state. The computations used the split-operator method with the fast Fourier transform, similar to that used in [18]. The chemical potentials are obtained by computing the net energy (the sum of kinetic, potential, self- and cross-nonlinear mean-field energies) for each component. We have chosen the wavefunctions $\psi_1(\boldsymbol{r},t)$ and $\psi_2(\boldsymbol{r},t)$ to be normalized to the number of particles in each component, so that $\int |\psi_i(\boldsymbol{r},t)|^2\,\mathrm{d}^3\boldsymbol{r} = N_i$. Choosing the symmetry of an initial configuration in the imaginary-time simulations, a solution $\psi_{1,2}(\boldsymbol{r})$ which minimizes the total energy

$$\mathcal{E} = \int \mathrm{d}^3\boldsymbol{r}\left[\mu_1|\psi_1(\boldsymbol{r},t)|^2 + \mu_2|\psi_2(\boldsymbol{r},t)|^2 - \tfrac{1}{2}U_{11}|\psi_1(\boldsymbol{r},t)|^4 - \tfrac{1}{2}U_{22}|\psi_2(\boldsymbol{r},t)|^4 - U_{12}|\psi_1(\boldsymbol{r},t)|^2|\psi_2(\boldsymbol{r},t)|^2\right] \quad (4)$$

within the class of functions possessing this symmetry can be found. The ground state of the two-component Hamiltonian is that with the smallest value of $\mathcal{E}$ for different symmetry classes.

3. Thomas–Fermi approximation

The TF approximation can be used to describe a zero-temperature condensate in the cases when the trapping-potential and mean-field nonlinear terms in GPEs are attractive and repulsive, respectively, and the number of atoms is large so that the mean-field energies are large compared with the kinetic energy. For the two-component system with overlapping wavefunctions,

$$\begin{pmatrix} \mu_1 - V_1(\boldsymbol{r}) \\ \mu_2 - V_2(\boldsymbol{r}) \end{pmatrix} = \begin{pmatrix} U_{11} & U_{12} \\ U_{21} & U_{22} \end{pmatrix} \begin{pmatrix} |\psi_1(\boldsymbol{r},t)|^2 \\ |\psi_2(\boldsymbol{r},t)|^2 \end{pmatrix} \tag{5}$$

where $U_{21} = U_{12}$. These equations can be solved as a linear system of equations for $|\psi_1(\boldsymbol{r},t)|^2$ and $|\psi_2(\boldsymbol{r},t)|^2$ in terms of the chemical potentials μ_1 and μ_2 to obtain

$$|\psi_1(\boldsymbol{r})|^2 = \frac{[\mu_1 U_{11} - \mu_2 U_{12}] - [U_{22} - U_{12}]\,(m/2)\omega^2 r^2}{U_{11}U_{22} - U_{12}U_{12}} \tag{6}$$

$$|\psi_2(\boldsymbol{r})|^2 = \frac{[\mu_2 U_{11} - \mu_1 U_{12}] - [U_{11} - U_{12}]\,(m/2)\omega^2 r^2}{U_{11}U_{22} - U_{12}U_{12}}. \tag{7}$$

The chemical potentials μ_1 and μ_2 are determined from the normalization conditions, $N_i = \int \mathrm{d}^D x\, |\psi_i(\boldsymbol{r},t)|^2$, where D is the dimension. We shall plot examples for $D = 1$, but our numerical method is valid for higher dimensions as well, hence we derive all the formulae for the general case.

When phase separation occurs and there are regions in the physical space occupied by one component only, the TF approximation leads, instead of equations (5), to the corresponding one-component TF equations. For example, if a phase with only species 1 exists in a particular region of space, an equation of the form

$$|\psi_1(\boldsymbol{r},t)|^2 = (\mu_1 - V_1(\boldsymbol{r}))/U_{11} \tag{8}$$

is to be used in this region. If another phase exists wherein species 1 and 2 are mixed, equations (5) are relevant for that region. The chemical potentials μ_1 and μ_2 must be determined by setting the number of atoms of each type equal to the integral of the corresponding density over the whole space.

Inspection of equations (5) suggests then that all the solutions can be classified according to the signs of three parameters: $\det U \equiv U_{11}U_{22} - (U_{12})^2$ and $\alpha_j \equiv U_{jj} - U_{12}$. In particular, $\alpha_{1,2}$ determine signs of the curvature (coefficients in front of r^2) of the *effective* quadratic potentials for the two components in equations (6) and (7). Qualitatively different types of possible states with overlapping wavefunctions (i.e. disregarding regions where only one of the species is present) identified by the TF analysis are defined in table 1.

Table 1. Classification of the Thomas–Fermi forms.

	$U_{11}U_{22} - U_{12}U_{12}$ $\equiv \det U$	$U_{11} - U_{12}$ $\equiv \alpha_1$	$U_{22} - U_{12}$ $\equiv \alpha_2$
Case 1 (type A)	Positive	Positive	Positive
Case 2 (type B)	Negative	Negative	Negative
Case 3 (type A)	Positive	Negative	Positive
Case 4 (type A)	Positive	Positive	Negative
Case 5 (type B)	Negative	Positive	Negative
Case 6 (type B)	Negative	Negative	Positive
Not possible	Positive	Negative	Negative
Not possible	Negative	Positive	Positive

Let us focus on those cases when the kinetic energy contribution does not change the general structure of the solution, but only generates narrow transient layers on the scale of the corresponding healing length, as in the single-component case when the TF approximation is valid (thus we consider large-size condensates). The analysis will include the TF configurations with and without overlap of the two different condensate wavefunctions. As already mentioned, in most cases both wavefunctions *do not overlap everywhere*, i.e. there is a region where only one wavefunction is different from zero. Consequently, a search for the lowest-energy state of the mixture cannot rely solely on equations (6) and (7) obtained with the assumption that the overlapping takes place everywhere.

Combining the cases represented in table 1 and single-wavefunction solutions within the TF approximation, we distinguish two general types of solutions: unseparated ones, having an overlap region where both wavefunctions are non-zero, and separated solutions which do not contain any overlap region. In the latter case, we shall see from the analysis of a full GP equation (with kinetic energy included) and also a *non-local* version of the two-species model, with a finite range of interatomic interactions, that it is necessary to further distinguish between weak ($U_{11}U_{22} \leqslant (U_{12})^2$) and strong ($U_{11}U_{22} \ll (U_{12})^2$) separation [9].

3.1. Partially overlapping wavefunctions ($U_{11}U_{22} - (U_{12})^2 > 0$)

In the case $\det U > 0$ (cases 1, 3 and 4 in table 1), we have checked numerically that the minimum-energy solution is given by the wavefunctions of the form shown in figure 1. Near the origin, both wavefunctions coexist up to the point where one of them vanishes. Past this point, one wavefunction vanishes, while the other one remains non-zero, following the single-component solution, equation (8). Figure 1 shows two different cases that are possible with the scenario described above. In figure 1(*a*), the two effective trapping potentials have the same sign of their curvature, i.e. $\alpha_1\alpha_2 > 0$, in the overlap region (this is case 1 in table 1). Figure 1(*b*) presents another situation, when the two effective potentials have opposite curvatures, $\alpha_1\alpha_2 < 0$ (these are cases 3 and 4 in table 1).

3.2. Separated wavefunctions ($U_{11}U_{22} - (U_{12})^2 < 0$)

This category is represented by cases 2, 5 and 6 from table 1. The simplest configuration is that with one wavefunction being different from zero in the region around the origin and vanishing beyond a separation radius, R, while the second component surrounds the first one. In this case, we can express μ_1 and μ_2 as functions of R and minimize the net free energy $\mathcal{E}$, in order to find the lowest eigenstate of this type. The normalization conditions for the wavefunctions of the two components give a set of relations between R, the chemical potentials μ_1 and μ_2, and the number of atoms in each condensate:

$$N_1 = \int_0^R \mathrm{d}^D r\,[\mu_1 - V(\boldsymbol{r})]/U_{11} \tag{9}$$

$$N_2 = \int_R^{R_0} \mathrm{d}^D r\,[\mu_2 - V(\boldsymbol{r})]/U_{22}. \tag{10}$$

Here $V(\boldsymbol{r})$ is the binding potential (3), and R_0 is an outer radius at which the wavefunction of the second component vanishes in the FT approximation. We first consider the 1D case and then show how these considerations can be generalized to two and three dimensions.

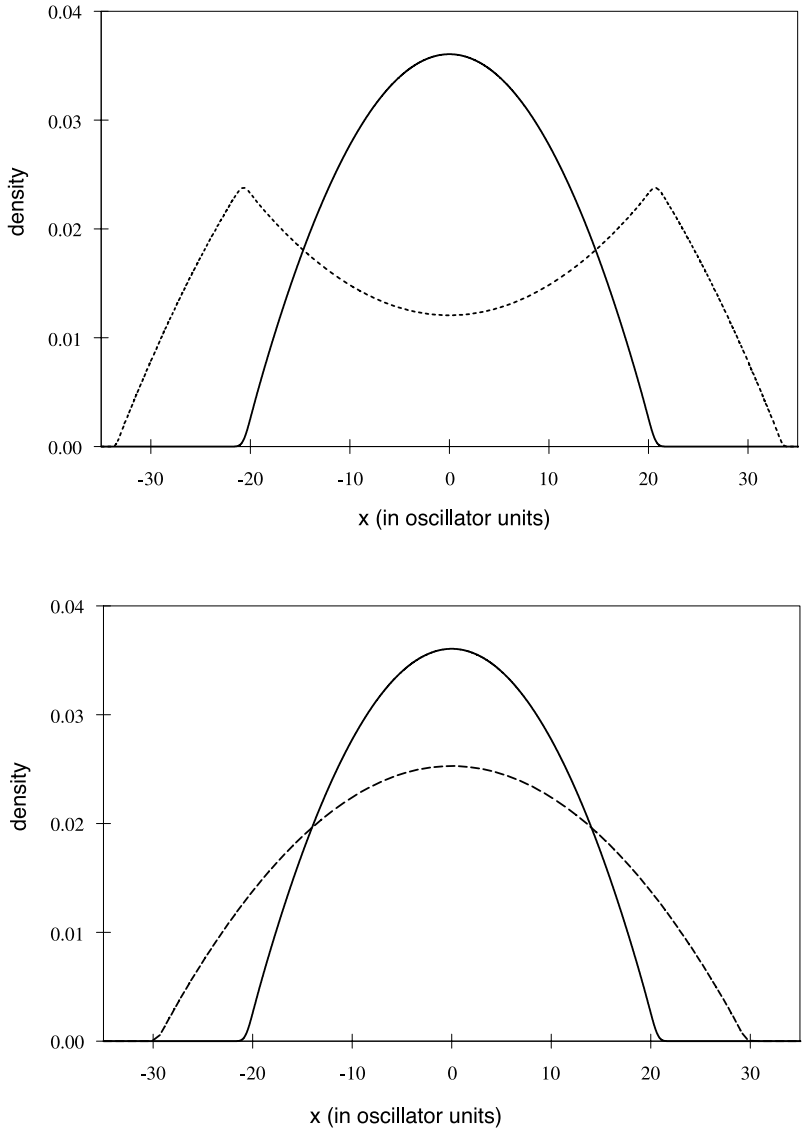

Figure 1. Two types of solutions with partial overlap. Densities for the first and the second component are plotted as full and broken curves. Panels (*a*) and (*b*) depict $U_{11} : U_{12} : U_{22} = 1.2 : 0.9 : 0.8$ and $U_{11} : U_{12} : U_{22} = 1.1 : 0.9 : 1$, respectively. In both panels $N_1 = N_2$. The oscillator length unit is given by $\sqrt{\hbar/m\omega}$. Density distributions in all figures are normalized to unity.

3.2.1. One-dimensional case. To find the value of the radius R minimizing $\mathcal{E}$, we solve the set of the coupled equations (9) and (10) for μ_1 and μ_2. The first equation can be solved directly to yield μ_1 as a function of R. The second equation is more complicated—it can be solved analytically only in the 1D and 2D cases, but not in 3D. In the 1D (3D) case, one needs to solve a third- (fifth-) order algebraic equation to find μ_2 as a function of R. The system of

equations (9) and (10) in 1D reduces to

$$2(\mu_1 R - \tfrac{1}{6}m\omega^2 R^3) = U_{11}N_1 \tag{11}$$

$$2\left(\frac{(2\mu_2)^{3/2}}{3\sqrt{m\omega^2}} - \mu_2 R + \frac{1}{6}m\omega^2 R^3\right) = U_{22}N_2. \tag{12}$$

In the case under consideration here, without spatial overlap of components, the total energy is simply a sum of the average values of the harmonic potential and half of the nonlinear term in the GP equation for each component state: $\mathcal{E} = \frac{1}{2}\sum_i \langle\psi_i|m\omega^2 x^2 + U_{ii}|\psi_i|^2/2|\psi_i\rangle$. If we substitute the direct expression for the wavefunction in the TF approximation we obtain

$$\mathcal{E} = \left(\frac{(2\mu_2)^{5/2}}{5\sqrt{m\omega^2}} - \mu_2^2 R + \frac{1}{20}(m\omega^2)^2 R^5\right)\Big/U_{22} + \left(\mu_1^2 R + \frac{1}{20}(m\omega^2)^2 R^5\right)\Big/U_{11} \tag{13}$$

and the chemical potentials can be found using equations (11) and (12).

3.2.2. Generalization to two and three dimensions. A particularly simple form of these equations is obtained upon introducing a TF radius $(R_{\mathrm{TF}})_{1,2}$ of the condensate in the corresponding dimension. The TF radius is defined as a radius of the *single* spherically symmetric condensate obtained in the TF approximation. We can find an explicit dependence between the chemical potentials of the condensates and the separation radius of the two phases in 2D. In this case, we again define the TF radii, which in 2D are equal to $(R_{\mathrm{TF}i})^4 = 8N_i U_{ii}/(\pi m\omega^2)$. In this case, we obtain the following set of equations for chemical potentials and total energy:

$$\mu_1 = \frac{m\omega^2}{4R^2}\left[(R_{\mathrm{TF1}})^4 + R^4\right] \tag{14}$$

$$\mu_2 = \frac{m\omega^2}{2}\left[(R_{\mathrm{TF2}})^2 + R^2\right] \tag{15}$$

$$\mathcal{E} = \frac{1}{(m\omega^2)^2}\left(\frac{2\mu_1^2 r^2 - \frac{1}{6}r^6}{R_{\mathrm{TF1}}^4} + \frac{\frac{8}{3}\mu_2^3 - 2\mu_2^2 r^2 + \frac{1}{6}r^6}{R_{\mathrm{TF2}}^4}\right) \tag{16}$$

where r is defined as $r = R\sqrt{m\omega^2}$.

In 3D we can define the TF radius given by $(R_{\mathrm{TF}i})\,5 = (15U_{ii})/(2\pi m\omega^2)$, and we can derive a set of equations which can be solved for the chemical potentials versus the separation radius:

$$\mu_1 = \frac{m\omega^2}{10R^3}\left[3R^5 + 2\,(R_{\mathrm{TF1}})^5\right] \tag{17}$$

$$4\left(\frac{2\mu_2}{m\omega^2}\right)^{5/2} + 3R^5 - 5\frac{2\mu_2}{m\omega^2}R^3 - 2\,(R_{\mathrm{TF2}})^5 = 0. \tag{18}$$

The energy is given in terms of the separation radius R by

$$\mathcal{E} = \frac{1}{(m\omega^2)^{5/2}}\left(\frac{\frac{5}{2}\mu_1^2 r^3 - \frac{15}{56}r^7}{R_{\mathrm{TF1}}^5} + \frac{\frac{5(2\mu_2)^{7/2}}{14} - \frac{5}{2}\mu_2^2 r^3 + \frac{15}{56}r^7}{R_{\mathrm{TF2}}^5}\right) \tag{19}$$

where $r = R\sqrt{m\omega^2}$.

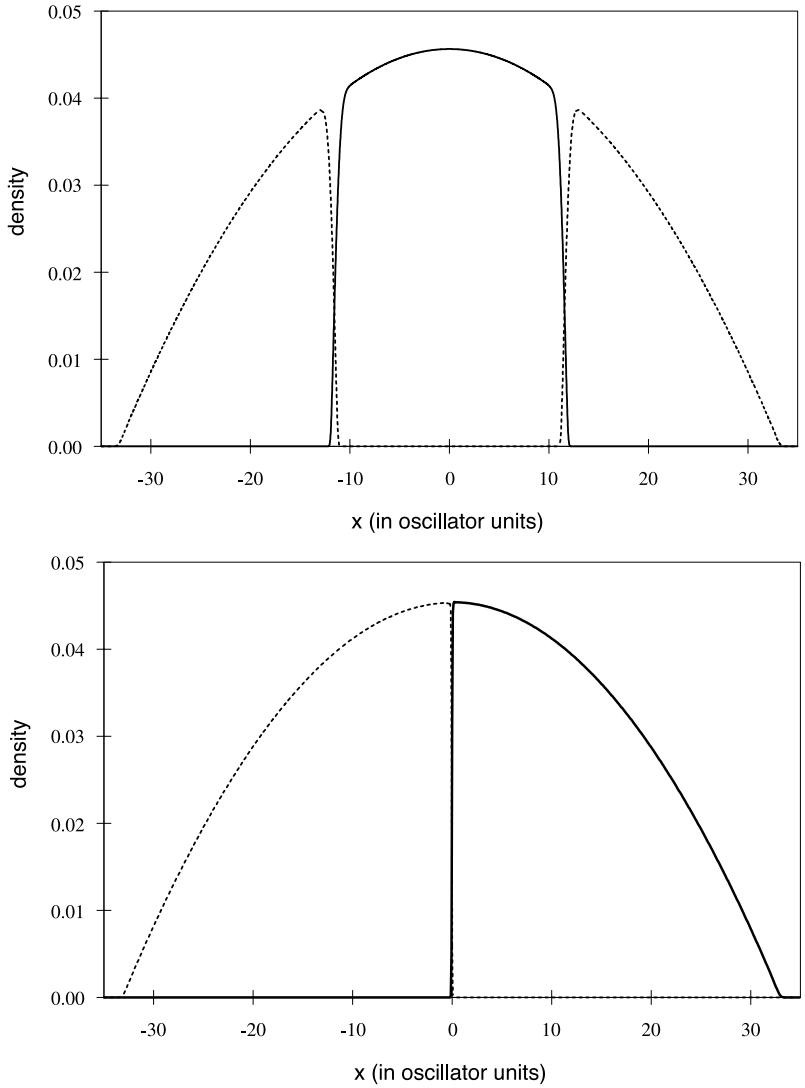

Figure 2. Two types of solutions without overlap: symmetric and asymmetric cases. Densities for the first and second components are plotted as full and broken curves. For both panels, the ratio of the scattering lengths is $U_{11} : U_{12} : U_{22} = 1 : 1.52 : 1.01$ and $N_1 = N_2$. The ratio of the energy of the asymmetric case to the symmetric one is 0.8.

3.2.3. Symmetry-breaking solutions. Eigenstates of the binary-condensate system that break the symmetry of the trapping potential exist. In 1D, a solution of this kind is given by TF parabolae that are stuck together. An example is shown in figure 2. In this case one can derive equations for μ_1 and μ_2 in the same way as in section 3.2.1, integrating the densities and substituting the result into the normalization conditions. The generalization to the dimensions higher than one may only be obtained if the separation surface (which reduces in 1D to a single

point) is simple. In 1D, the corresponding coupled equations take the form

$$\frac{(2\mu_1)^{3/2}}{3\sqrt{m\omega^2}} - \mu_1 R + \frac{1}{6}m\omega^2 R^3 = U_{11}N_1 \tag{20}$$

$$\frac{(2\mu_2)^{3/2}}{3\sqrt{m\omega^2}} + \mu_2 R - \frac{1}{6}m\omega^2 R^3 = U_{22}N_2 \tag{21}$$

$$\mathcal{E} = \left(\frac{(2\mu_1)^{5/2}}{5\sqrt{m\omega^2}} - \mu_1^2 R + \frac{1}{20}(m\omega^2)^2 R^5\right)\Big/ U_{11} + \left(\frac{(2\mu_1)^{5/2}}{5\sqrt{m\omega^2}} + \mu_2^2 R - \frac{1}{20}(m\omega^2)^2 R^5\right)\Big/ U_{22}. \tag{22}$$

We have checked numerically that this solution cannot give rise to a minimum of the free energy, hence, within the framework of the FT approximation, the ground state cannot be the one with broken symmetry. The difference in the energy between symmetric and asymmetric cases is usually very small making them almost degenerate. The degeneracy is exact in the limit when $U_{11} \to U_{22}$ and is removed by the kinetic energy.

4. The role of kinetic energy

In this section we present the results of our studies of the contribution of the kinetic energy to the total energy and on the functional dependence of the ground state of the binary mixtures of the BEC. For a single condensate, in the regime of the validity of the TF approximation, the kinetic energy creates a healing length, ξ, in the region where the condensate wavefunction tends to zero. This healing length is of the order of $(8\pi na)^{-1/2}$ [19], where a is a scattering length and n is an average density of the condensate. For the binary mixtures of BECs there are two length scales that can be defined in order to characterize two kinds of boundary regions. One is the ordinary healing length of a single condensate and refers to the healing of the wavefunction outside the region of coupled wavefunctions. However, for mixtures another region between the two components exists and a penetration depth, χ, as a length scale over which two components overlap. The penetration depth is a function of $\det U$. For $\det U < 0$ the lowest-energy state consists of partially overlapping wavefunctions; hence the penetration depth is of the order of the size of the condensate. With decreasing $\det U$ the penetration depth becomes smaller and goes to zero in the limit of strong repulsion as $\det U \to -\infty$. At the same time, the contribution of the kinetic energy to the total energy becomes more important, in spite of the shrinking overlap region. This situation is illustrated in figure 3. The energy of the lowest eigenstate is plotted in the symmetric and asymmetric classes as a function of $\det U/(U_{11}U_{22})$. In figure 3 only one curve is plotted for $\det U > 0$ where the contribution of the kinetic energy is negligible and the Thomas–Fermi approximation gives an excellent prediction for both the value of the ground state energy and its wavefunction. As the value of $\det U$ becomes negative, the lowest-energy state within a TF approximation consists of two separated components and the energy does not depend on U_{12} and is plotted as a horizontal broken line in figure 3. For $\det U < 0$ the contribution of the kinetic energy is substantial and it is larger for the symmetric case which has two interfaces between phases. The asymmetric configuration has only one interface in the lowest-energy state. Hence, the ground state loses symmetry of the trap.

In order to search for stable symmetry-breaking solutions we kept N_1, U_{11} and U_{12} constant and varied N_2 and U_{22}. Figure 4 plots the ratio of the total energy in the asymmetric case to the energy of the symmetric one as a function of these two variables. Almost all solutions are symmetry-breaking ones and a trough is formed near $U_{22} = U_{11}$. The trough is an optimal region for finding symmetry-breaking solutions.

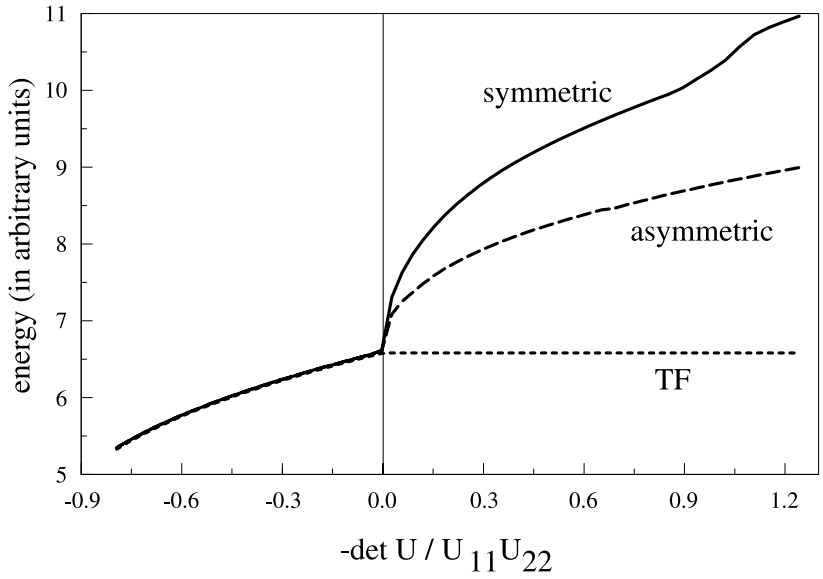

Figure 3. Total energy versus the dimensionless quantity det $U/(U_{11}U_{22})$ for the symmetric and asymmetric cases (numerical simulation) and the TF prediction. Here $N_1 = N_2$, U_{11} and U_{22} are kept constant (the same as in figure 2) whereas U_{12} is varied. For arguments smaller than zero the three curves are indistinguishable.

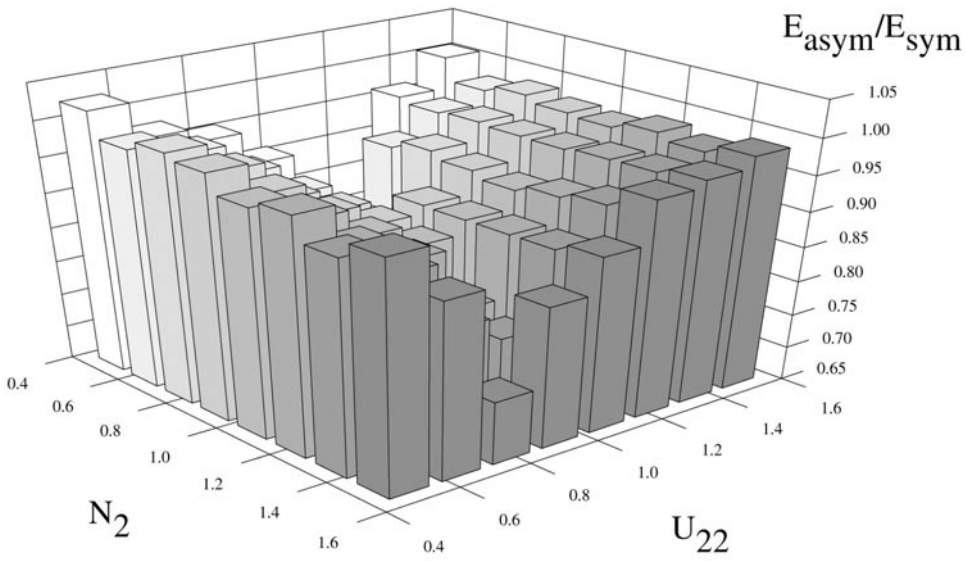

Figure 4. Ratio of the total energy of the asymmetric case to the corresponding value in the symmetric phase versus U_{22} and N_2 scaled by certain initial values. The initial values are the same as in figure 2 (i.e. $U_{11} : U_{12} : U_{22} = 1 : 1.52 : 1.01$ and $N_1 = N_2$). Note the deep valley near $U_{11} = U_{22}$.

5. Finite-interaction range

So far we have considered the mean-field description of a BEC mixture assuming a zero-range delta-function pseudopotential. It is of interest to consider the effects of a finite-range

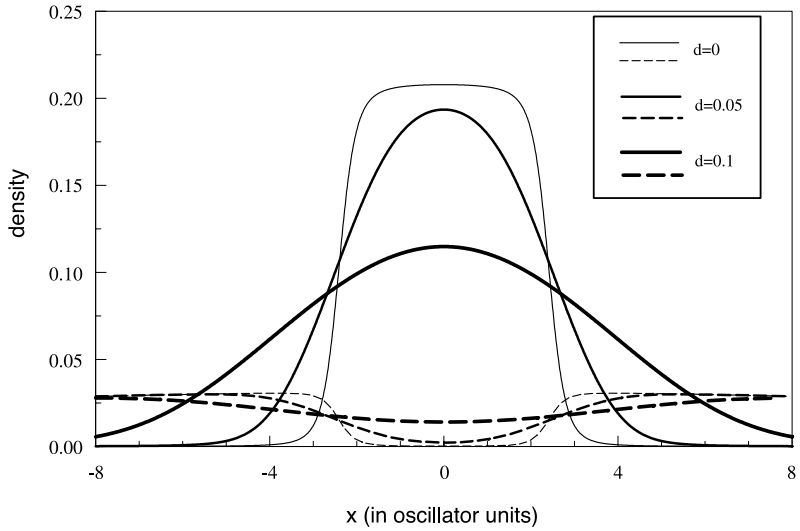

Figure 5. Dependence of the density distributions of a two-component BEC in weakly segregated phases on the range of the intercomponent interaction d. Here $U_{12} = 1.02U_{11} = 1.02U_{22}$ and $N_2/N_1 = 0.15$. The effect of attenuation of the interaction with growth of the range is illustrated for three values of d.

interatomic interaction on the ground-state structure in the two-component condensate. We introduce a pseudopotential in the form of a normalized Gaussian with a finite width (i.e. range) which recovers the zero-range limit result as the range vanishes. We search for changes in the structure of the ground state of the two-component system as the range of the *intercomponent* interactions only are varied, keeping the delta-function pseudopotential for the self-interactions. The results displayed below were obtained by means of direct numerical simulations, not the FT approximation. In 1D, the intercomponent-interaction terms in equations (1) $U_{12}|\psi_i(x,t)|^2$ are replaced by a non-local expression,

$$U_{12}\frac{1}{\sqrt{2\pi d^2}}\int_{-\infty}^{+\infty} \mathrm{d}y\ \exp\left(\frac{-(x-y)^2}{2d^2}\right)|\psi_i(y,t)|^2 \tag{23}$$

where d is the interaction range. The Gaussian form was chosen to model a finite-range potential solely for its simplicity (see also [20] for the role of a finite interaction range in attractive single-component BEC within this model). This family of finite-range potentials has a constant scattering length within the first Born approximation. All the cases that we investigate below correspond to configurations with *separated* wavefunctions in the usual TF limit (see section 3.2).

5.1. Weak separation ($U_{11}U_{22} \leqslant (U_{12})^2$)

Here we discuss case 2 of table 1. Figure 5 shows the overlap region between the wavefunctions of the two components; this overlap region grows as the interaction range increases. Starting from relatively well separated phases, we end up with a complete overlap of the two components (i.e. the component located initially outside the narrow-width component finally penetrates it). The intercomponent interaction parameters are chosen as $U_{12} = 1.02U_{11} = 1.02U_{22}$, which places this case not far from the boundary between the cases of separated and overlapping phases. In other words, increasing the interaction range forces a transition from separated

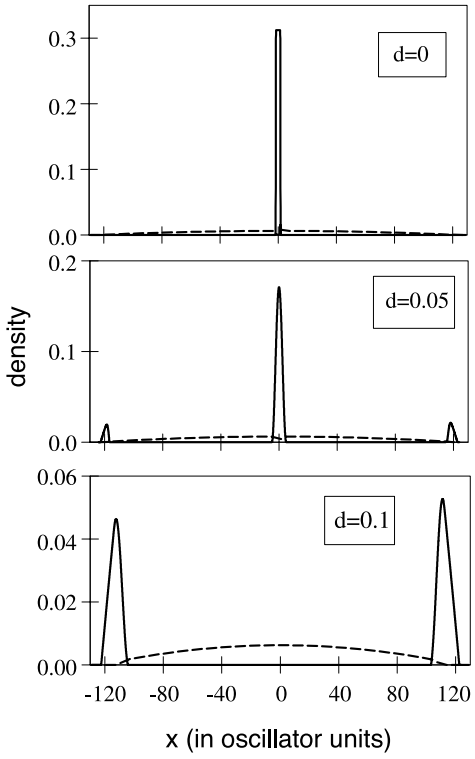

Figure 6. Interaction-range-induced change of the ground-state density distribution of a two-component BEC in weakly segregated phases, but with a large disparity in the number of atoms in the components. The parameters are $U_{12} = 1.01U_{11} = 1.01U_{22}$ and $N_2/N_1 = 0.02$.

phases to penetrating ones. Within the zero-range model, this would correspond to a transition from $U_{12} \geqslant \sqrt{U_{11}U_{22}}$ to $U_{12} \leqslant \sqrt{U_{11}U_{22}}$, i.e. to attenuation of the interaction. A simple argument justifies this conclusion. Suppose the interaction range is so large that the long-range potential varies only slightly over the extent of the interface between the nearly separated components (where the intercomponent interaction is important). Then, the interaction terms of equation (23) would be approximately constant, producing only a shift in the total energy of the mixture, but not affecting the shape of the two wavefunctions. When d becomes comparable to the penetration depth (see also [9]), phase separation is reduced. This is clearly illustrated in figure 5.

Although the parameters in the 1D solution are not directly relevant to an experimental situation, we decreased the range of the intercomponent interactions so that they are in a realistic range of values. From the aforementioned arguments, we see that in order to observe a difference from the zero-range case, the interaction range should be comparable to the penetration depth. In order for the interaction range to be small and yet correspond to the boundary between overlapping and segregated phases, a large disparity in the number of atoms in the two components is required. This situation is depicted in figure 6, where $U_{12} = 1.01U_{11} = 1.01U_{22}$, but $N_1 \gg N_2$. We observe a qualitative change in the ground-state solution: the component that initially was at the centre of the trap moves to its outskirts as the interaction range grows. Although $d = 0.1\sqrt{\hbar/m\omega}$ (bottom frame in figure 6) would usually correspond to several tens of nanometres, we argue that one can optimize the sensitivity to d by considering the regime of parameters near the boundary between the penetrating and segregated phases. The possibility of manipulating the strength of atomic collisions is not excluded, as Feshbach resonances have been observed in BEC samples [21], and several other

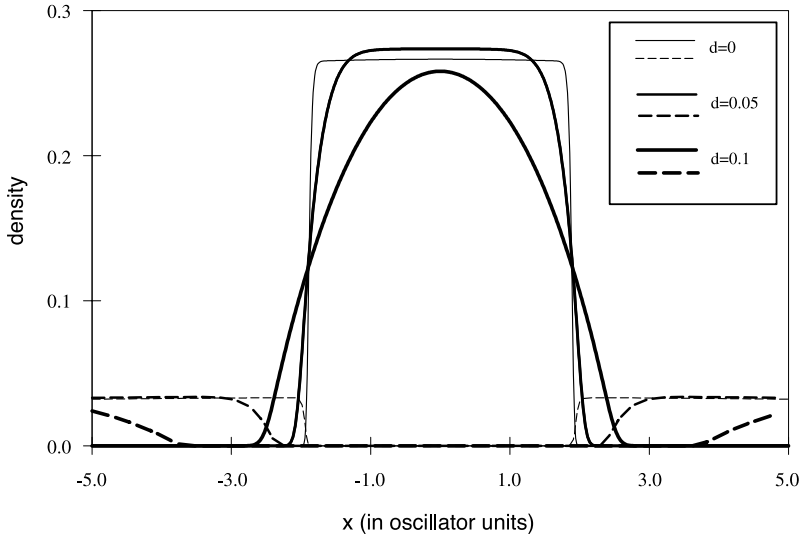

Figure 7. Enhanced mutual repulsion as an effect of a finite interaction range between strongly separated phases. Here $U_{11} : U_{12} : U_{22} = 1 : 7 : 1$ and $N_2/N_1 = 8$.

proposals in this respect have been put forward [22, 23]. Using such techniques one could vary the intercomponent scattering length in order to scan the region near $\det U = 0$. Then, by comparing the measured structure of the mixture to the predictions of the two theoretical models (i.e. those with zero and finite interaction range) one could determine the effective range of interactions (which is a parameter in the latter model). Thus, one can probe the microscopic parameter d via a magnified effect such as the qualitative change of the condensate structure from separated phase to penetrating phase.

5.2. Strong separation ($U_{11}U_{22} \ll (U_{12})^2$)

In the preceding section we demonstrated the effective attenuation of the mean-field repulsive interaction between two components of a BEC due to an increase in the range of the interaction for the case when $U_{11}U_{22} \leqslant (U_{12})^2$. Now we turn to the case when the parameters of the BEC mixture are far from threshold for the onset of the penetrating phase. In figure 7 the parameters are $U_{12} = 7U_{11} = 7U_{22}$, hence the interface between the two components is very sharp. Since now it is much easier to match the range of interactions with the penetration depth, one might expect that effects similar to those described above will appear at even smaller values of d. However, this is not the case. The mutual repulsion of the components remains very strong even if reduced by a finite interaction range. As the interaction range increases, the two components tend to move apart, yielding two completely separated phases.

6. Summary and conclusion

We have presented a detailed classification of stable solutions for binary mixtures of dilute atomic condensates. The analysis is particularly simple within the Thomas–Fermi approximation. Within this approximation one can distinguish two general classes of ground state for two-component condensate mixtures: unseparated ones with an overlap region (both component wavefunctions are simultaneously non-zero) and separated ones not containing

an overlap region (except for the tail penetration). The latter also contains solutions that do not possess the symmetry of the trapping potential. Components are separated if $\det U \equiv U_{11}U_{22} < U_{12}^2 < 0$ and they overlap if $\det U > 0$. The predictions from the TF approximation become ambiguous in the region of parameters where phase-separated solutions which break the symmetry of the trap are energy-degenerate with the phase-separated solutions preserving the symmetry. In this case, it is crucial to include the contribution of the kinetic energy operator and of the mutual interaction energy in determining the structure of the ground state geometry, which tend to favour the asymmetric solutions. The physical reason for this is probably a smaller interface region in the asymmetric solutions. It is these interface regions which contribute most to both the kinetic and mutual interaction energies. We have carried out our numerical calculations in 1D, but our conclusions should be valid in two and three dimensions as well. The condensates, if not overlapping, should have a propensity towards states with minimal interface surface area. In the $\det U < 0$ case, with kinetic energy included, we further recognize a weak separation regime ($\det U \leqslant 0$) and a strong separation regime ($\det U \ll 0$) when the penetration depth goes to zero. The contribution of the kinetic energy to the total energy increases with decreasing $\det U$ (for negative $\det U$), in spite of the decreasing interface size (see figure 3). This is due to the increasing importance of the U_{12} term that gives the cross-interaction energy of atoms from different components.

Since the size of the overlap region can be very small (smaller than a single condensate healing length), it is of interest to investigate the possible impact of a small, but non-zero, interaction range in a binary condensate. We have developed a model of a finite-range potential by introducing a pseudopotential in the form of a normalized Gaussian with finite width. We identified two distinctly different cases. In one case, that of significant overlap, the finite range tends to increase the penetration over the delta function interaction, and in the other, that of strong separation, the finite range leads to a trough between the two condensates.

Acknowledgments

We thank M Gajda and J Mostowski for stimulating discussions. This work was supported in part by the Polish KBN grant no 2PO3B07819 (MT), the US–Israel Binational Science Foundation and the James Franck Binational German–Israel Program in Laser–Matter Interaction (YBB). KR and KG acknowledge the support of the subsidy from the Foundation for Polish Science and of the Polish KBN grant no 203B05715. Part of the results have been obtained using computers at the Interdisciplinary Center for Mathematical and Computational Modelling (ICM) at Warsaw University.

References

[1] Ho T L and Shenoy V B 1996 *Phys. Rev. Lett.* **77** 3276
[2] Esry B D, Greene C H, Burke J P and Bohn J L 1997 *Phys. Rev. Lett.* **78** 3594
[3] Pu H and Bigelow N P 1998 *Phys. Rev. Lett.* **80** 1130
[4] Öhberg P 1999 *Phys. Rev.* A **59** 634
[5] Esry B D 1998 *Phys. Rev.* A **58** R3399
Esry B D and Greene C H 1999 *Phys. Rev.* A **59** 1457
Timmermans E 1998 *Phys. Rev. Lett.* **81** 5718
Chui S T and Ao P 1999 *Phys. Rev.* A **59** 1473
[6] Law C K, Pu H, Bigelow N P and Eberly J H 1998 *Phys. Rev.* A **58** 531
[7] Law C K, Pu H, Bigelow N P and Eberly J H 1997 *Phys. Rev. Lett.* **79** 3105
[8] Williams J, Walser R, Cooper J, Cornell E and Holland M 1999 *Phys. Rev.* A **59** R31

[9] Ao P and Chui S T 1998 *Phys. Rev.* A **58** 4836
[10] Öhberg P and Stenholm S 1998 *Phys. Rev.* A **57** 1272
Öhberg P and Stenholm S 1997 *J. Phys. B: At. Mol. Opt. Phys.* **30** 2749
[11] Myatt C J *et al* 1997 *Phys. Rev. Lett.* **78** 586
Hall D S *et al* 1998 *Phys. Rev. Lett.* **81** 1539
Hall D S, Matthews M R, Wieman C E and Cornell E A 1998 *Phys. Rev. Lett.* **81** 1543
[12] Stamper-Kurn D M *et al* 1998 *Phys. Rev. Lett.* **80** 2027
[13] Trippenbach M, Band Y B and Julienne P S 2000 *Phys. Rev.* A **62** 023608
(Trippenbach M, Band Y B and Julienne P S 2000 *Preprint* cond-mat/0002119)
[14] Molmer K 1998 *Phys. Rev. Lett.* **80** 1804
[15] Burke J P, Bohn J L, Esry B D and Greene C H 1998 *Phys. Rev. Lett.* **80** 2097
[16] Drummond P D, Kheruntsyan K V and He H 1998 *Phys. Rev. Lett.* **81** 3055
[17] Malomed B A *et al* 1997 *Phys. Rev.* E **56** 4725
[18] See, for example, Agarwal G P 1995 *Nonlinear Optics* (New York: Academic)
Trippenbach M and Band Y B 1997 *Phys. Rev.* A **56** 4242
Trippenbach M and Band Y B 1998 *Phys. Rev.* A **57** 4791
[19] Dalfovo F, Giorgini S, Pitaevskii L P and Stringari S 1999 *Rev. Mod. Phys.* **71** 463
[20] Parola A, Salasnich L and Reatto L 1998 *Phys. Rev.* A **57** R3180
Pérez-García V M, Konotop V V and García-Ripoll J J 1999 *Preprint* cond-mat/9912301
[21] Inouye S *et al* 1998 *Nature* **392** 151
[22] Fedichev P O, Kagan Yu, Shlyapnikov G V and Walraven J T M 1996 *Phys. Rev. Lett.* **77** 2913
Marinescu M and You L 1998 *Phys. Rev. Lett.* **81** 4596
[23] Goldstein E V, Moore M G, Pu H and Meystre P 2000 *Preprint* cond-mat/0005025